This project is part of the PRIMA Programme supported by the European Union

RESERVOIR

Sustainable groundwater RESources managEment by integrating eaRth observation deriVed monitoring and flOw modelIng Results

PRIMA

GA no. 1924

DELIVERABLE D3.1

A-DInSAR processing in Alto Guadalentín aquifer (Spain)

Author(s):	IGME: Guadalupe Bru, Carolina Guardiola Albert, Pablo Ezquerro, Marta Béjar UNIPV: Roberta Bonì, Claudia Meisina UNIPD: Pietro Teatini UA: Roberto Tomás DEU: Alper Elçi UJ: Khaldoun Shatanawi
Responsible Partner:	IGME
Version:	V3
Date:	29/12/20
Distribution Level (CO, PU)	PU

Acknowledgement

This project has received funding from the Partnership for Research and Innovation in the Mediterranean Area under the European Union's Horizon 2020 research and innovation programme under grant agreement No 1924. We thank the European Union Copernicus program and the European Space Agency for access to Sentinel-1 data. This project was carried out using CSK® Products, © ASI (Italian Space Agency), delivered under an ASI licence to use: ASI Project Science Id 408 "Study of surface deformation due to groundwater exploitation in southern Spain".

Statement of originality

This document contains original unpublished work except where clearly indicated otherwise. Acknowledgement of previously published material and of the work of others has been made through appropriate citation, quotation or both.

DOCUMENT REVISION HISTORY

Date	Version	Editor	Comments	Status
16/12/2020	1.0	Guadalupe Bru y Carolina Guardiola Albert (IGME)		1st ver
21/12/2020	1.0_RT	Roberto Tomás Jover (UA)		Draft
21/12/2020	1.0_PT	Pietro Teatini (UNIPD)		Draft
22/12/2020	1.0_MBP	Marta Béjar Pizarro (IGME)		Draft
22/12/2020	1.0_AE	Alper Elçi (DEU)		Draft
22/12/2020	1.0_CM	Claudia Meisina (UNIPV)		Draft
23/12/2020	1.0_UJ	Khaldoun Shatanawi (UJ)		Draft
23/12/2020	1.0_RB	Roberta Boni (UNIPV)		Draft
23/12/2020	2.0	Guadalupe Bru y Carolina Guardiola (IGME)	New section	Draft
28/12/2020	2.0_MBP_PE	Marta Béjar, G. Bru, Pablo Ezquerro (IGME)		Draft
29/12/2020	3.0	Carolina Guardiola Albert (IGME)		Final

LIST OF PARTNERS

Participant	**Name**	**Country**
UNIPV	Università degli Studi di Pavia	Italy
UNIPD	Università di Padova	Italy
IGME	Instituto Geológico y Minero de España	Spain
UA	Universidad de Alicante	Spain
DEU	Dokuz Eylul University	Turkey
UJ	The University of Jordan	Jordan
CER	Consorzio di Bonifica di secondo grado per il Canale Emiliano Romagnolo	Italy
RSCN-AWR	Royal Society for the Conservation of Nature - Azraq Wetland Reserve	Jordan

GLOSSARY

Acronym	Description
A-DInSAR	Advanced Differential Interferometric Synthetic Aperture Radar
ASI	Agenzia Spaziale Italiana
CNR	Italian National Research Council
CPT	Coherence Pixel Technique
CSK	Cosmo-SkyMed satellite
DEM	Digital Elevation Model
DInSAR	Differential Interferometric Synthetic Aperture Radar
DS	Distributed Scatters
EO	Earth Observation
ESA	European Space Agency
EW	Extra Wide Swath
GEP	Geohazards Exploitation Platform
G-POD	Grid Processing on Demand
GSNL	Geohazard Supersites and Natural Laboratory
IGN	Spanish National Geographic Institute
IREA	Institute for the Electromagnetic Sensing of the Environment
IW	Interferometric Wide Swath
LOS	Line of Sight of the satellite
MoD	Italian Ministry of Defense
MUR	Italian Ministry of Research
NAVSTAR	NAVigation System Time and Ranging
PO	Project Objectives
P-SBAS	Parallel Small BAseline Subset

Acronym	Description
PS	Persistent Scatterers
RSLab	Remote Sensing Laboratory
S-1	Sentinel-1 satellite
SAR	Synthetic-aperture radar
SBAS	Small BAseline Subset
SLC	Single Look Complex
StaMPS	Stanford Method for Persistent Scatterers
StaMPS/MTI	Stanford Method for Persistent Scatterers Multi-Temporal
TS	Time Series
UPC	Universitat Politecnica de Catalunya
UNAVCO	University NAVSTAR Consortium
WP	Work Package

CONTENTS

LIST OF FIGURES AND TABLES

1. INTRODUCTION, GOAL AND PURPOSE OF THIS DOCUMENT

The aim of RESERVOIR project is to provide new products and services for a sustainable groundwater management model to be developed and tested in four water-stressed Mediterranean pilot sites and then be applicable in other regions via an interdisciplinary approach.

The specific Project Objectives (PO) are the following:

- PO1. Develop an innovative methodology for the hydrogeological characterization of large-scale aquifer systems using low-cost and non-intrusive data such as satellite-based Earth Observation (EO) techniques.
- PO2. Integrate advanced EO techniques into numerical groundwater flow and geomechanical models to improve the knowledge about the current capacity to store water and the future response of aquifer systems to natural and human-induced stresses.
- PO3. Enhance the knowledge about the impacts of agricultural and tourism activities on the water resources by quantifying the ground deformation during the monitored periods.
- PO4. Engage water management authorities and provide models for an optimal management of the aquifer systems. We will engage 4 water authorities in 4 different countries through a series of face-to-face workshops (each participant will organize at least 1 workshop in the first 4 months of the project). The water authorities will be involved in the conceptualization and design of guidelines for Groundwater Resource Management (GRM). Best practices of water management for agricultural and tourism purposes will be developed taking advantage of the knowledge and methodologies from the outputs of PO1, PO2 and PO3.
- PO5. Dissemination and exchange of the generated knowledge among the experts and the managers in charge of land and groundwater management in the pilot sites to strengthen the aquifer resilience.

The objective of WP3 is the processing (using A-DInSAR techniques) of SAR images acquired by the Sentinel-1 radar satellite constellation in representative areas of each pilot site. As far as the SAR image processing execution allows it, the definition of the representative area will try to include the area of the groundwater numerical model. These Earth Observation (EO) techniques can provide surface displacements time series caused by terrain deformation, such as land subsidence processes. The terrain displacement data will be used to improve the conceptual and physical groundwater flow models and to calibrate the deformation model of each of the studied aquifers. These activities will be performed to achieve PO1 and PO2.

For the A-DInSAR processing, the coherent pixel technique (CPT) (Blanco-Sanchez et al., 2008; Mallorquí et al., 2003) developed by the Remote Sensing Laboratory (RSLab) at Universitat Politecnica de Catalunya (UPC) and provided by Dares Technology, will be used. Additionally, the InSAR processing tools of the Geohazards Exploitation Platform (GEP) funded by the European Space Agency, will be used for a first assessment of ground deformation in each pilot site.

The WP3 is subdivided in four tasks, corresponding to the EO processing of each pilot site:

- T3.1 – A-DInSAR processing in Alto Guadalentín aquifer (Spain)
- T3.2 – A-DInSAR processing in the coastal aquifer of Comacchio (Italy)

- T3.3 – A-DInSAR processing in Gediz River Basin (Turkey)
- T3.4 – A-DInSAR processing in Azraq Wetland Reserve (Jordan)

In this deliverable, a detailed description of A-DInSAR processing in Alto Guadalentín aquifer (Spain) is given. Additionally, a brief introduction to the A-DInSAR technique using Sentinel-1 images and the results of T3.1 are presented.

2. A-DInSAR

2.1 Sentinel-1 SAR data

A Synthetic Aperture Radar (SAR) is an active microwave sensor which provides radar images at high spatial resolution. It can be mounted on a spaceborne platform acquiring data regardless of the weather. These spaceborne sensors operate day and night in a quasi-polar orbit, either ascending (south - north) or descending (north - south). Since the early 90s, several SAR satellites with ever-improving imaging characteristics have been launched by an international community of satellite providers, collectively ensuring continuous coverage of the Earth with SAR data (Flores-Anderson et al., 2019). The characteristic bands at which SAR satellites operates are L-band, C-band and X-band (Figure 2.1), with wavelengths of 23.6, 5.6 and 3.1 cm, respectively. With moderate- to high-resolution capabilities and increased vegetation penetration, C-band data can be seen as a good compromise between X-band and the longer wavelength L-band sensor classes to monitor areas with low to moderate vegetation.

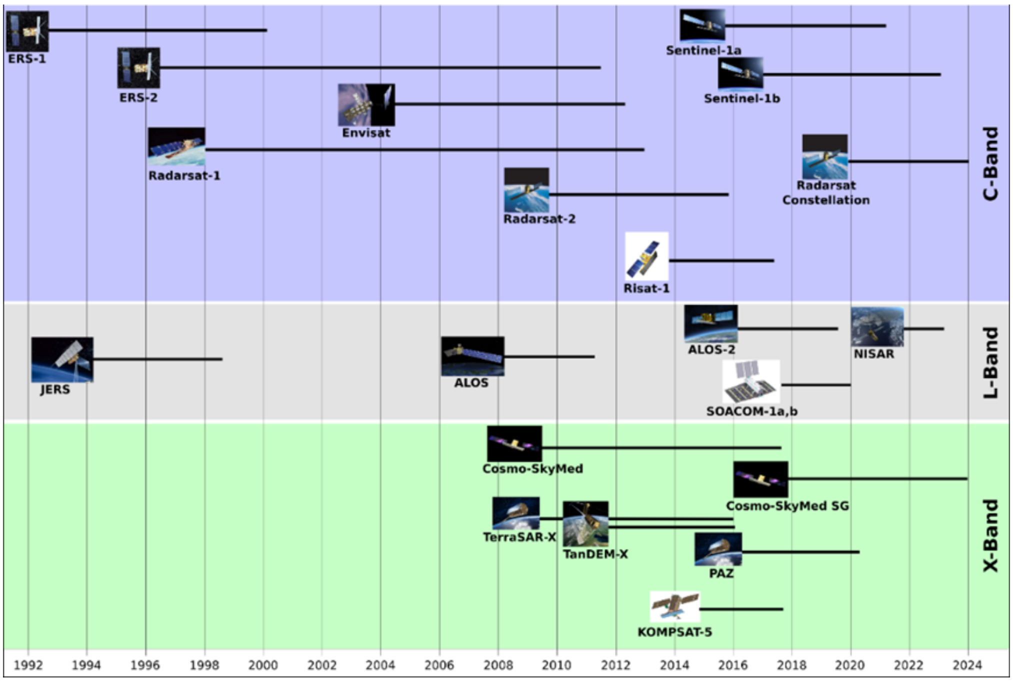

Figure 2.1 Chart of past, present and upcoming SAR satellite missions operating at L-band, C-band and X-band (UNAVCO, web).

Among the C-band spaceborne sensors, the Sentinel-1 (S-1) mission from the European Space Agency (ESA) comprises a constellation of two polar-orbiting satellites (Figure 2.2) that were launched in 2014 (Sentinel-1A) and 2016 (Sentinel-1B). They are expected to transmit Earth observation data for at least 7 years and have fuel on-board for 12 years. Two other spacecraft (Sentinel-1C and Sentinel-1D) are planned to replace the first two satellites at the end of their operational lifespan. The mission is designed to provide enhanced revisit frequency, coverage, timeliness and reliability for operational services and applications requiring long time series (ESA-web). As part of Copernicus, that is the European Union's Earth Observation Programme, the Sentinel-1 mission adopted a free, full, and open data policy to all users for the S-1 data products via Copernicus Open Access Hub (https://scihub.copernicus.eu/). Further details of the sensor properties can be found in Table 2.1 (Flores-Anderson et al., 2019).

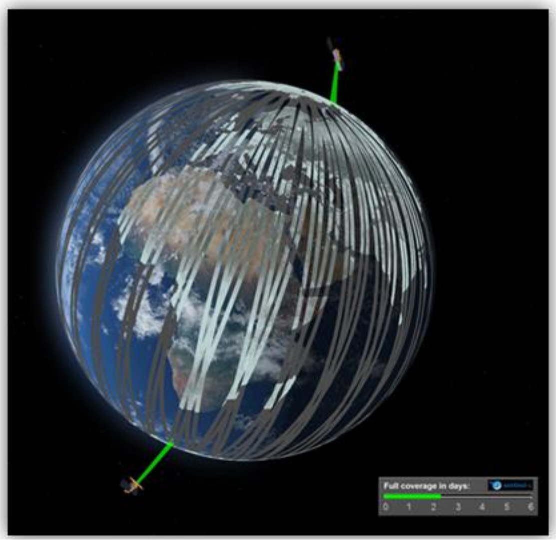

Figure 2.2 S-1 constellation.

Table 2.1 Sentinel-1 spaceborne SAR sensor properties.

Lifetime	2014-present
Wavelength	C-band (λ = 5.6 cm)
Polarization	Single: HH, VV Dual: HH/HV, VV/VH
Resolution	Stripmap: 5x5m Interferometric Wide Swath (IW): 5x20 m Extra Wide Swath (EW): 20-40 m
Frame size	Stripmap: 375 km IW: 250 km EW: 400 km
Repeat cycle (revisit period)	Satellite: 12 days Constellation: 6 days
Data access	Free & open via Copernicus Open Access Hub

2.2 A-DInSAR processing

Satellite radar differential interferometry (DInSAR) is a geodesic technique, with cloud penetrating and day-night operational capabilities, that allows to remote sense small displacements of the terrestrial surface by analysing the phase differences between pairs of single look complex (SLC) SAR images.

Thanks to the availability of large SAR data archives, a stack of independent interferograms can be created from various SAR images of the same illuminated area. This allows to reconstruct displacement time series from selected point scatterers (PS) or distributed scatterers (DS) that are above a phase stability threshold in all the interferograms, using the so-called multitemporal or Advanced Differential radar interferometry (A-DInSAR) algorithms. Typically, a minimum of 15-20 images is needed to perform an A-DInSAR analysis with C-band (Crosetto et al., 2016), although it is possible to use shorter datasets with X-band due to the higher resolution and the shorter wavelength of this band (Bovenga et al., 2012). In any case, the larger the number of available scenes, the better the quality of the deformation velocity and time series estimation. There are two methods to create the stack of interferograms. The first one uses a single reference SAR image (Single master) so the number of interferograms will be N–1, where N is the number of SAR images. The second one uses a small baseline configuration, where a denser interferogram network is created linking multiple SAR images (Multi-master). The criterion to select the punctual targets in the interferograms can be simplified in amplitude and coherence methods. Amplitude selection methods work at full resolution and limit the interferometric processing only to those pixels that behave consistently over a long period of time (PS). Coherence based methods use distributed scatters (DS), or in other words, areas whose scatter properties are not altered with time, which requires a multilook that lowers the resolution. A comparison of different A-DInSAR algorithms can be found in (Crosetto et al., 2016; Osmanoğlu et al., 2016) and (Minh et al., 2020).

Any A-DInSAR algorithm dealing with data stacks, requires a number of conceptual steps that have to be sequentially performed (Casu et al., 2014). These are the SAR image focusing (if raw data is used, not needed in SLC images), the SAR image co-registration using a Digital Elevation Model (DEM), the interferogram generation, the unwrapping of the computed phases and the retrieval of the final displacement time-series. A simplified block diagram of A-DInSAR algorithms is shown if Figure 2.3 (De Luca et al., 2015).

The Small BAseline Subset (SBAS) approach (Berardino et al., 2002) is a seminal work that proposes a complete advanced DInSAR procedure using small baselines to limit the spatial decorrelation, multilooked data to reduce phase noise and a coherence based selection criterion. To deal with the current scenario characterized by huge SAR archives relevant to the present and future SAR missions, a parallel computing solution for the SBAS processing chain (P-SBAS) was developed (Casu et al., 2014). This step forward in optimizing computing performance was particularly suitable for web service implementation and handling big data volumes. Indeed, the P-SBAS algorithm was integrated within the Grid Processing on Demand (G-POD) environment by CNR IREA into the ESA's Geohazards Exploitation Platform (GEP). The developed on-demand web tool, which is specifically addressed to scientists that are non-expert in DInSAR data processing, permits to set up an efficient on-line P-SBAS processing service to produce surface deformation mean velocity maps and time series in an unsupervised manner (De Luca et al., 2015). The G-POD strategy is to co-locate both DInSAR algorithms and computational resources close to the SAR data archives, as well as to provide the capability to easily generate the DInSAR results in a friendly interface. The concept "unsupervised" stands for the fact that the P-SBAS processing chain runs automatically in G-POD without user interaction. The efficiency and robustness of the chain guarantee the achieved result accuracy. The P-SBAS web tool on G-POD requires a mandatory registration step on the ESA web portal (http://gpod.eo.esa.int/), by creating an ESA Earth Observation Single Sign-On (EO-SSO). For a detailed description of the steps refer to G-POD user manual in http://wiki.services.eoportal.org/tiki-index.php?page=GPOD+User+Manual.

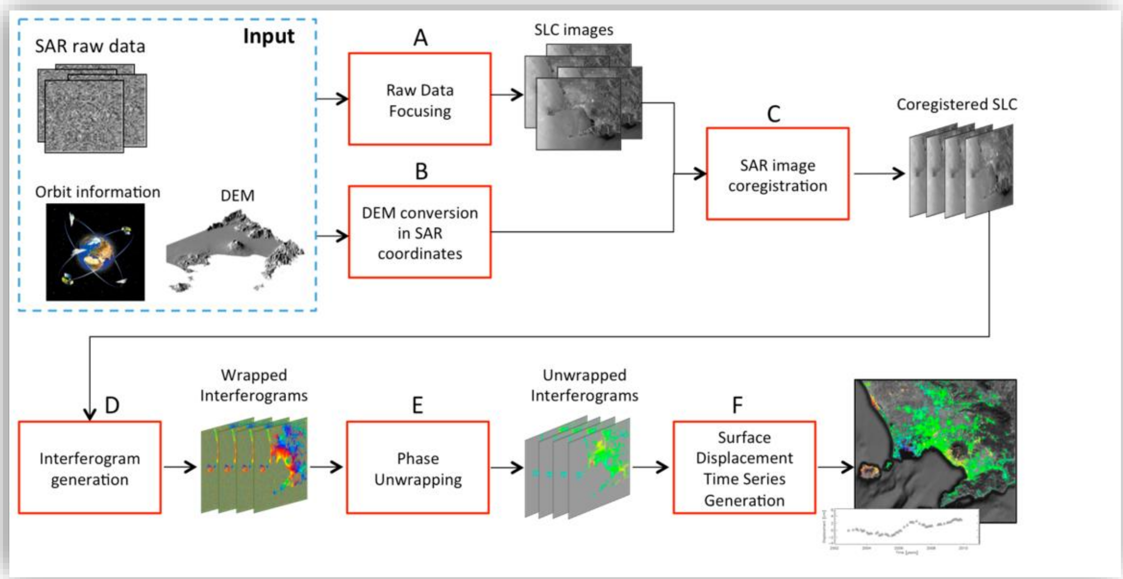

Figure 2.3 Simplified block diagram of A-DInSAR algorithm steps (De Luca et al., 2015).

The Coherent Pixels Technique (CPT) is a A-DInSAR algorithm with a similar approach to SBAS based on multilook imagery. It was developed by the Remote Sensing Laboratory (RSLab) at Universitat Politecnica de Catalunya (UPC) (Blanco-Sanchez et al., 2008; Mora et al., 2003). It is updated to S-1 TOPS acquisition system (Centolanza et al., 2017). The CPT is divided into two main steps. The PRISAR processing step generates the co-registered images, interferograms, coherence maps and differential interferograms. SUBSOFT module is responsible for the processing of the Advanced DInSAR products, the estimation of linear and non-linear deformation components and geocoding results.

3 S-1 DATASET AND PROCESSING DESCRIPTION OF THE STUDIED AREA

3.1 Preliminary regional processing with GEP

A preliminary A-DInSAR processing has been performed using the P-SBAS interferometry chain implemented in GEP tool at a regional scale. This unsupervised procedure is intended to identify potential deformation areas before carrying out a more refined InSAR analysis with the CPT technique over those areas. A brief description of the dataset, processing and results are described below.

A total of 79 S-1 SAR images in IW mode were acquired from 16/07/2017 to 02/11/2018 (Table 3.1) in descending orbit (track 8), covering an extensive area of about 13,000 km^2 which includes almost the full extent of the Alto Guadalentín basin (Figure 3.1). A multilook factor of 5 × 20 was applied, which lowered the spatial resolution to 90 m. The unsupervised processing detected 974,008 pixels (Figure 3.2). The output clearly detects maximum deformation at the north of the Alto Guadalentín basin, with maximum velocities around -8 cm/year in the LOS direction (movement away from the satellite). Based on these preliminary results, the CPT analysis, centered in the Alto Guadalentín ground deformation area and with better spatial resolution, was performed (section 3.2).

Table 3.1 Dates of S-1 SAR images used for GEP processing in yyyymmdd format.

Image	Date	Image	Date	Image	Date	Image	Date
1	20170722	21	20171113	41	20180313	61	20180717
2	20170722	22	20171119	42	20180319	62	20180723
3	20170728	23	20171125	43	20180325	63	20180729
4	20170803	24	20171201	44	20180331	64	20180804
5	20170809	25	20171207	45	20180406	65	20180810
6	20170815	26	20171213	46	20180418	66	20180816
7	20170821	27	20171219	47	20180424	67	20180822
8	20170827	28	20171225	48	20180430	68	20180828
9	20170902	29	20171231	49	20180506	69	20180903
10	20170908	30	20180106	50	20180512	70	20180909
11	20170914	31	20180112	51	20180518	71	20180915
12	20170920	32	20180118	52	20180524	72	20180921
13	20170926	33	20180124	53	20180530	73	20180927
14	20171002	34	20180130	54	20180605	74	20181003
15	20171008	35	20180205	55	20180611	75	20181009
16	20171014	36	20180211	56	20180617	76	20181015
17	20171020	37	20180217	57	20180623	77	20181021
18	20171026	38	20180223	58	20180629	78	20181027
19	20171101	39	20180301	59	20180705	79	20181102
20	20171107	40	20180307	60	20180711		

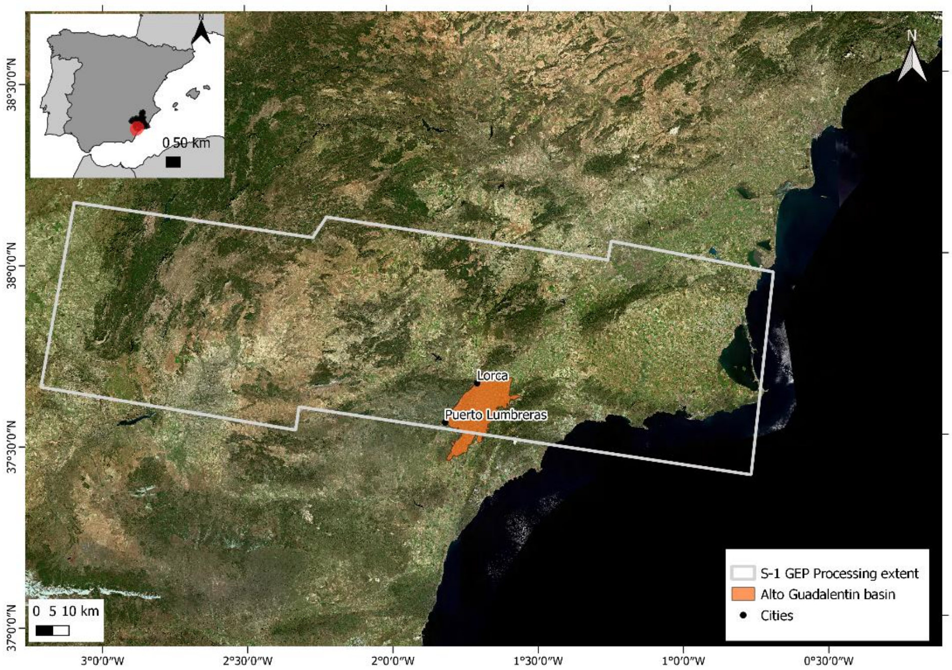

Figure 3.1 Location of the studied area and S-1 SAR dataset extent processed with GEP.

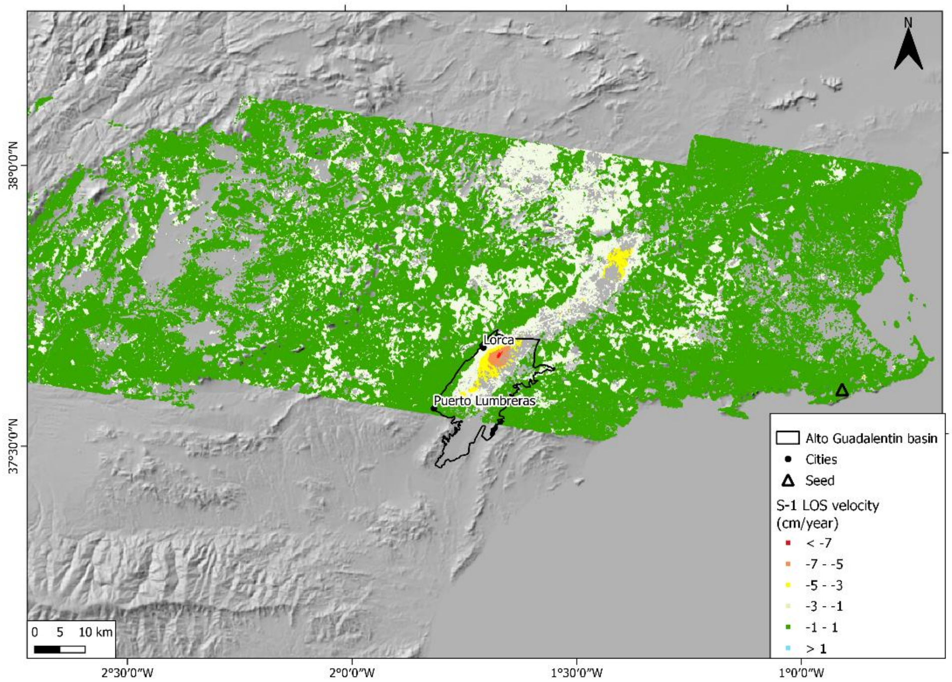

Figure 3.2 LOS displacement velocity in the study area for the S-1 dataset processed with P-SBAS in the GEP. Period July 2017 to November 2018.

3.2 Pilot site A-DInSAR processing

For the A-DInSAR processing in the Alto Guadalentín aquifer pilot site (Spain), the coherent pixel technique (CPT) has been applied. A stack of 37 S-1 SAR images, acquired from October 2014 to July 2016 in descending orbit and covering almost the full extent of the Alto Guadalentín basin were used (Figure 3.3). A list of the acquisition dates of the images is shown in Table 3.2. The maximum temporal baseline is 192 days allowing a low temporal decorrelation in the interferograms. Maximum perpendicular baseline is 185 m. The specific parameters of the S-1 dataset can be found in Table 3.3.

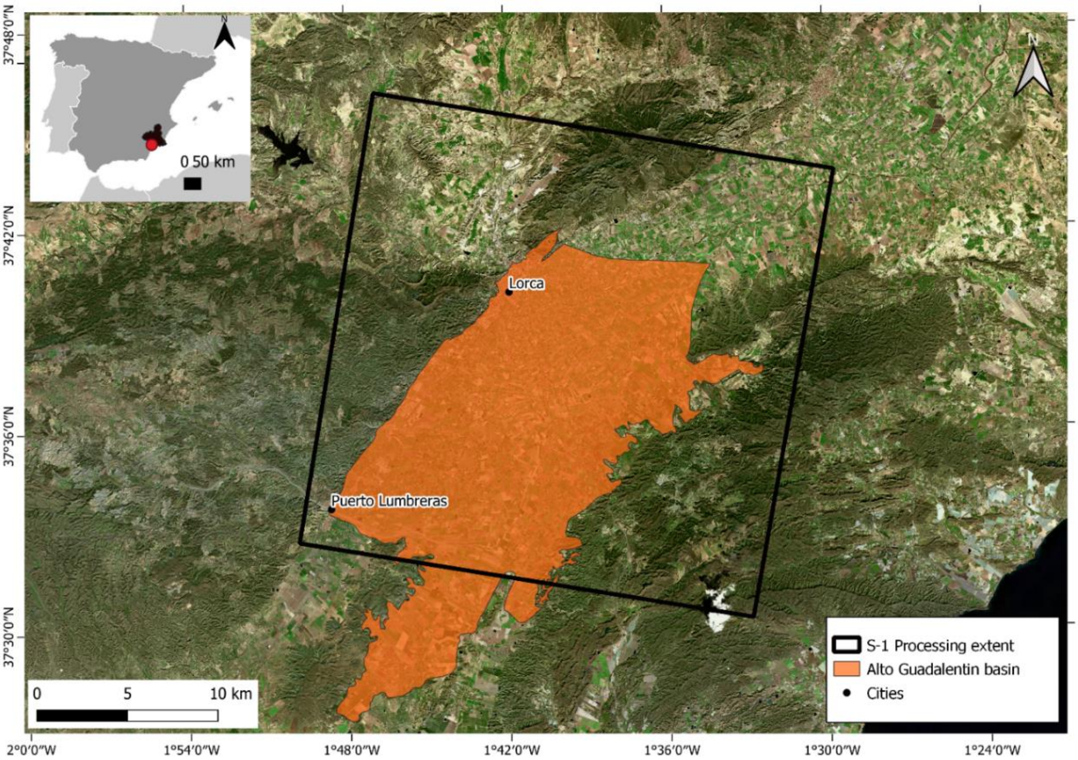

Figure 3.3 Location of the studied area and S-1 SAR dataset extent processed with CPT.

Table 3.2 Dates of S-1 SAR images used for CPT processing in yyyymmdd format.

Image	Date	Image	Date	Image	Date	Image	Date
1	20141030	11	20150603	21	20151001	31	20160329
2	20141123	12	20150615	22	20151013	32	20160410
3	20141205	13	20150627	23	20151212	33	20160422
4	20150227	14	20150709	24	20151224	34	20160504
5	20150311	15	20150721	25	20160105	35	20160516
6	20150323	16	20150802	26	20160117	36	20160528
7	20150404	17	20150814	27	20160129	37	20160703
8	20150416	18	20150826	28	20160210		
9	20150428	19	20150907	29	20160305		
10	20150522	20	20150919	30	20160317		

Table 3.3 S-1 dataset parameters.

Number of images	37
Initial date	30/10/2014
Final date	03/07/2016
Acquisition mode	Wide Swath (IW)
Orbit	Descending
Track	8
Incidence angle of the area of interest [º]	between 37.54º and 39.08º (medium-east side of the second swath in descending orbit direction)
Minimum revisit period [days]	12
Max. temporal baseline [days]	192
Max. spatial baseline [m]	185
Wavelength (λ) [cm]	5.6
Polarization	VV

S-1 SAR images were processed using CPT. This Small Baseline approach is suited for the studied area, due to the predominance of agricultural land cover and the lack of good scatters out of the urban areas. To remove the topographical contribution, a 25 m resolution Digital Elevation Model (DEM) from the Spanish National Geographic Institute (IGN) was used. A total of 206 interferograms were generated using a multilook of 3 × 11 designed to generate a near-squared pixel with good resolution (about 45 m). The Distributed Scatters (DS) approach was used for the pixel selection where the Line of Sight (LOS) velocities and time series were estimated. This kind of approach fits especially well with S-1 characteristics, allowing the detection of a good point density in agricultural areas. In the initial coherent pixel candidate selection, a coherence threshold of 0.3 was selected. The reference stable point (seed) is located in the stable mountainous areas that surround the basin. The processing of SAR data from the S-1 descending track, covering an area of 625 km^2, produced 206,530 DS. The coherent pixels were mainly concentrated over urban and not vegetated areas (Ezquerro et al., 2020). Specific processing data is summarized in Table 3.4.

Table 3.4 A-DInSAR processing parameters and results.

Number of interferograms	206
Covered Area [km²]	625
Multilook (Az × Rg)	3 × 11
Number of DS	206,530
DS density [DS per km²]	330

4 DELIVERED S-1 MAP DESCRIPTION

The delivered map consists in a shape file with the fields listed in Table 4.1:

- Shapefile with the A-DInSAR results (DS points):
  - LorcaP1_velin_LOS.cpg = specification of the codepage for identifying the character set to be used (optional file).
  - LorcaP1_velin_LOS.dbf = dBASE table that stores the attribute information of features (Table 3.1).
  - LorcaP1_velin_LOS.prj = coordinate system information, **projected WGS 84 / UTM zone 30N.**
  - LorcaP1_velin_LOS.shp = the shapefile itself.
  - LorcaP1_velin_LOS.shx = index file that stores the index of the feature geometry.

Table 4.1 Fields included in the attribute table of the shapefile (LorcaP1_velin_LOS.dbf).

Field	Description
ID	Identification number for each DS
Range	Radar image columns
Azimuth	Radar image row
Lon [º]	WGS84 Geographic Longitude
Lat [º]	WGS84 Geographic Latitude
UTM_E [m]	UTM East
UTM_N [m]	UTM North
Height [m]	Height above mean sea level
GROUND_HEI [m]	DEM error (altitude difference between reference DEM and the one calculated during the processing)
RATE [cm/year]	Velocity in LOS (negative values indicate movement away from the satellite)
QUALITY	Spatial coherence of the DS (minimum was set to 0.3)
Yyyymmdd [cm]	Deformation value at date yyyymmdd (negative values indicate movement away from the satellite)

A QGIS project, with additional files and a layout template, is also delivered:

- S-1_Lorca.qgz: QGIS project with the same specific format for future deliverables is the following (the paths to the files will need to be specified when opening in other folder locations):
    - Coordinate system: projected WGS 84 / UTM zone 30N
    - Layers:
        - LorcaP1_velin_LOS.shp = DS points with graduated simbology
        - RefPoint.shp = reference point or seed
        - Cities_AltoGuadalentin.shp = location of Lorca and Puerto Lumbreras
        - AltoGuadalentin.shp = aquifer boundary
        - PNOA_MDT05_ETRS89_HU30_big.asc = DEM 5m LIDAR PNOA merge of sheets 0953, 0954, 0975, 0976, 0997, 0997B downloaded from http://centrodedescargas.cnig.es/CentroDescargas/index.jsp.
        - Hillshade.tif = raster effect from PNOA_MDT05_ETRS89_HU30_big.asc
        - pnt_sentinel2_2020_winter_naturalcolor_AltoGuadalentin.tif = orthophoto of the studied area, clipped from original downloaded from http://centrodedescargas.cnig.es/CentroDescargas/index.jsp.
    - Layout_Sentinel1_velocity_LOS.qpt = layout template.

5 ADDITIONAL PROCESSING

For the Alto Guadalentín pilot site, in addition to the Sentinel-1 data analysis, we have performed an A-DInSAR analysis with CPT using CosmoSkyMed (CSK) SAR data. The main advantage of having this extra information is the longer time span of deformation data to be related to piezometric level change (activities in WP4), to better characterize the hydrogeological model of the aquifer system (activities in WP5) and the deformation model (activities in WP6). Moreover, there is the possibility of decomposing the LOS displacements into up-down and east-west components from ascending CSK and descending S1 data, which overlap in time, by interpolating the displacement rate to a common resolution grid (Ezquerro et al., 2020).

CSK is a 4-spacecraft constellation launched in 2007, where each satellite is equipped with a SAR instrument. It was conceived by ASI (Agenzia Spaziale Italiana), and funded by the Italian Ministry of Research (MUR) and the Italian Ministry of Defense (MoD), Rome, Italy. Their antennas operate at a X band (λ = 3.5 cm) and the spatial resolution can reach ≤1m in the Spotlight mode, 3 to 15m in Stripmap mode and up to 100m in ScanSAR mode. The nominal incidence angles (where the system grants the image quality requested) vary between 20° and 59°. One of the main advantages offered by the four spacecrafts is the high revisit frequency; each satellite has a repeat cycle of 16 days that can be reduced to hours by combining data from the constellation. The access to CSK data is commercial and images of a particular area can be acquired under request. However, there are special pricing conditions and freely available areas (GSNL supersites) for institutional and scientific users.

5.1 CSK dataset and processing description of the studied area

A package of 114 CSK SAR images were used. They were acquired from June 2011 to December 2016 in ascending orbit and covering almost the full extent of the Alto Guadalentín basin (Figure 5.1). A list of the acquisition dates of the images was shown in Table 5.1. Due to extremely high temporal resolution of CSK constellation (maximum revisit time of 4 days) (Covello et al., 2010) a regular 16 days temporal sampling was selected in order to reduce processing machine-time costs. Spatial amplitude and temporal evolution of the studied phenomenon render the processing of the complete catalogue unnecessary and the selected gap between images is short enough to reduce temporal decorrelation. Specific CSK dataset parameters can be found in Table 5.2 (Ezquerro et al., 2020).

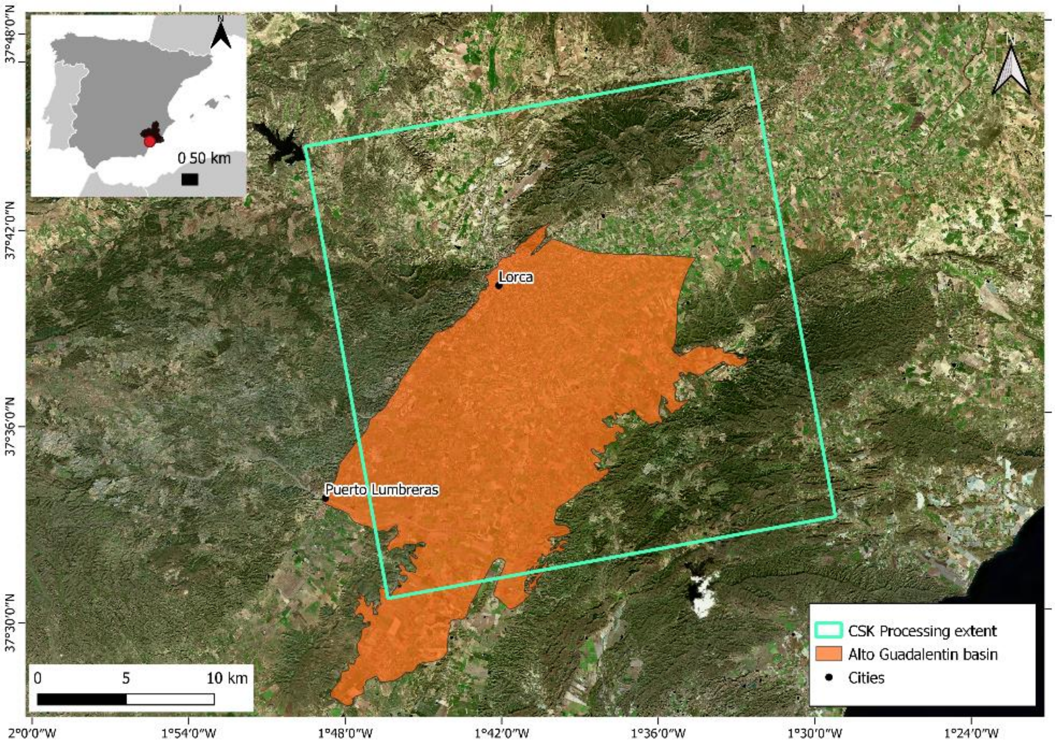

Figure 5.1 Location of the studied area and CSK SAR dataset extent processed with CPT.

Table 5.1 Dates of CSK SAR images in yyyymmdd format.

Image	Date	Image	Date	Image	Date	Image	Date
1	20110602	30	20121127	59	20140322	87	20150613
2	20110618	31	20121213	60	20140423	88	20150715
3	20110704	32	20121229	61	20140509	89	20150727
4	20110717	33	20130118	62	20140521	90	20150816
5	20110805	34	20130203	63	20140606	91	20151003
6	20110821	35	20130211	64	20140622	92	20151015
7	20110906	36	20130219	65	20140716	93	20151019
8	20110922	37	20130303	66	20140728	94	20151104
9	20111008	38	20130323	67	20140817	95	20151120
10	20111024	39	20130408	68	20140829	96	20151206
11	20111109	40	20130503	69	20140914	97	20151222
12	20111125	41	20130522	70	20140930	98	20160107
13	20111211	42	20130607	71	20141012	99	20160120
14	20120112	43	20130623	72	20141029	100	20160208
15	20120128	44	20130709	73	20141117	101	20160228
16	20120210	45	20130725	74	20141129	102	20160308
17	20120229	46	20130810	75	20141219	103	20160311
18	20120316	47	20130826	76	20150101	104	20160412
19	20120401	48	20130911	77	20150117	105	20160428
20	20120417	49	20130927	78	20150217	106	20160511
21	20120503	50	20131013	79	20150221	107	20160530
22	20120519	51	20131029	80	20150305	108	20160615
23	20120604	52	20131114	81	20150325	109	20160701
24	20120722	53	20131130	82	20150406	110	20160730
25	20120823	54	20131220	83	20150410	111	20160814
26	20120908	55	20131229	84	20150426	112	20160831
27	20120924	56	20140117	85	20150512	113	20161103
28	20121010	57	20140129	86	20150528	114	20161205
29	20121026	58	20140306				

Table 5.2 CSK dataset parameters.

Number of images	114
Initial date	02/06/2011
Final date	05/12/2016
Acquisition mode	Stripmap-Himage (STR-HIMAGE)
Orbit	Ascending
Incidence angle of the area of interest [º]	43.16º
Minimum revisit period [days]	3
Max. temporal baseline [days]	269
Max. spatial baseline [m]	488
Wavelength (λ) [cm]	3.5
Polarization	HH

CSK SAR images were also processed using CPT. A total of 323 interferograms were generated using a multilook of 5 × 5, which produced nearly squared pixels with good resolution (about 25 m). The Distributed Scatters (DS) approach was used for the pixel selection where the Line of Sight (LOS) velocities and time series were estimated. In the initial coherent pixel candidate selection, a coherence threshold of 0.45 was selected. The reference stable point (seed) is the same that for S-1, located in the stable mountainous areas that surround the basin. The processing of SAR data from the CSK ascending track, covering an area of 676 km^2, produced a higher DS density than the S-1 dataset (422,458 DS). Also for this dataset, the coherent pixels were mainly concentrated over urban and not vegetated areas (Ezquerro et al., 2020). Specific processing data is summarized in Table 5.3.

Table 5.3 A-DInSAR CSK processing parameters.

Number of interferograms	323
Covered Area [km^2]	676
Multilook (Az × Rg)	5 × 5
Number of DS	422,458
DS density [DS per km^2]	625

5.2 Delivered CSK map description

The delivered map consists of a shape file with the fields listed in Table 5.4.:

- Shapefile with the A-DInSAR results (DS points):
    - Lorca_CSK_velin_LOS.cpg = specification of the codepage for identifying the character set to be used (optional file).
    - Lorca_CSK_velin_LOS.dbf = dBASE table that stores the attribute information of features (Table 5.4).
    - Lorca_CSK_velin_LOS.prj = coordinate system information, **projected WGS 84 / UTM zone 30N.**
    - Lorca_CSK_velin_LOS. shp = the shapefile itself.
    - Lorca_CSK_velin_LOS.shx = index file that stores the index of the feature geometry.

Table 5.4 Fields included in the attribute table of the shapefile (Lorca_CSK_velin_LOS.dbf).

Field	Description
ID	Identification number for each DS
Range	Radar image columns
Azimuth	Radar image row
Lon [º]	WGS84 Geographic Longitude
Lat [º]	WGS84 Geographic Latitude
UTM_E [m]	UTM East
UTM_N [m]	UTM North
Height [m]	Height above mean sea level
GROUND_HEI [m]	DEM error (altitude difference between reference DEM and the one calculated during the processing)
RATE [cm/year]	Velocity in LOS (negative values indicate movement away from the satellite)
Yyyymmdd [cm]	Deformation value at date yyyymmdd (negative values indicate movement away from the satellite)

A QGIS project, with additional files and a layout template, is also delivered:

- CSK_Lorca.qgz: QGIS project with the same specific format for future deliverables is the following (the paths to the files will need to be specified when opening in other location):
    - Coordinate system: projected WGS 84 / UTM zone 30N
    - Layers:
        - Lorca_CSK_velin_LOS.shp = DS points with graduated symbology.
        - RefPoint.shp = reference point or seed. Same one for S-1.
        - Cities_AltoGuadalentin.shp = location of Lorca and Puerto Lumbreras.
        - AltoGuadalentin.shp = aquifer boundary.

- PNOA_MDT05_ETRS89_HU30_big.asc = DEM 5m LIDAR PNOA merge of sheets 0953, 0954, 0975, 0976, 0997, 0997B downloaded from http://centrodedescargas.cnig.es/CentroDescargas/index.jsp
- Hillshade.tif = raster effect from PNOA_MDT05_ETRS89_HU30_big.asc
- pnt_sentinel2_2020_winter_naturalcolor_AltoGuadalentin.tif = orthophoto of the studied area, clipped from original downloaded from http://centrodedescargas.cnig.es/CentroDescargas/index.jsp

- Layout_CSK_velocity_LOS.qpt = layout template.

6 ANALYSIS OF RESULTS

6.1 S-1 Analysis results

Figure 6.1 shows the InSAR map of deformation rates derived from S-1 processing with CPT. The measurements are in LOS with an angle of ~38º from the normal to the Earth surface. The ±1 cm/year stability threshold is based on the standard deviation values estimated for all the DS in a stable area. Previous InSAR studies over this area revealed that radar noise over this area is usually high and stability thresholds around ±1 cm/year are consistently used (Bonì et al., 2015). The maximum deformation area is located in the northern section of the basin and the maximum deformation rate detected in LOS was –7.5 cm/year. There is a local maximum located at the SW of the basin towards Puerto Lumbreras. If only vertical displacement is considered, the vertical projected maximum velocity rises up to -9.7 cm/year (Ezquerro et al., 2020). The deformation pattern coincides spatially with other monitoring data, such as CSK, ALOS-PALSAR and ENVISAT (Béjar-Pizarro et al., 2016; Bonì et al., 2015). In particular, the additional processing of CSK data is presented in the following sections. Figure 6.1 shows the classification of the average LOS velocity in the period from October 2014 to July 2016. Representative TS are shown in Figure 6.2. TS extracted from the S-1 dataset present a relatively high instability especially in the areas with low deformation due to the short-processed time-span.

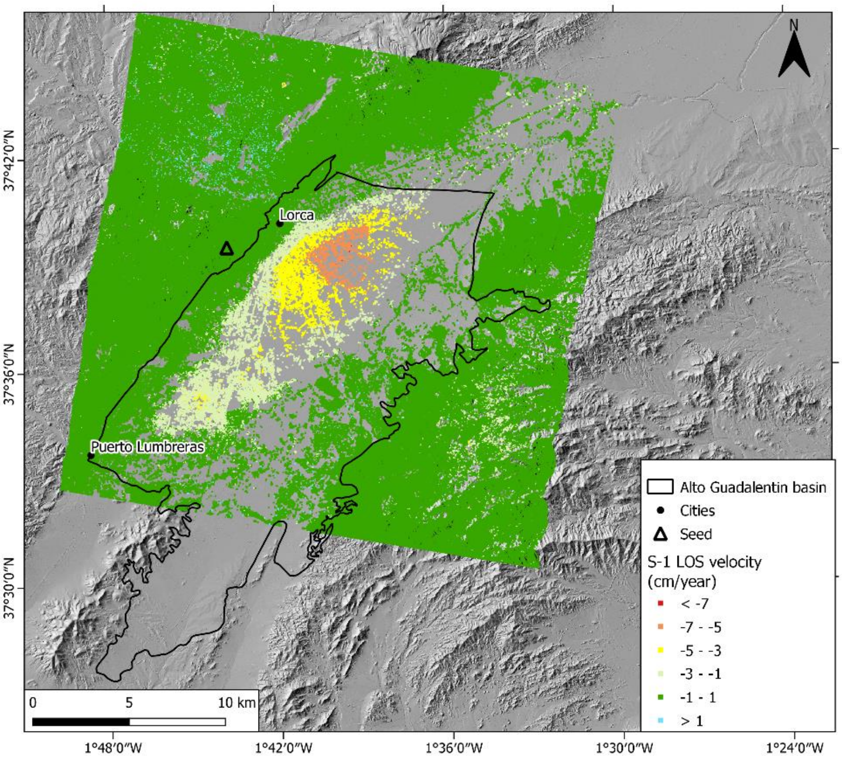

Figure 6.1 LOS displacement velocity in the study area for the S-1 dataset processed with CPT. Period October 2014 to July 2016.

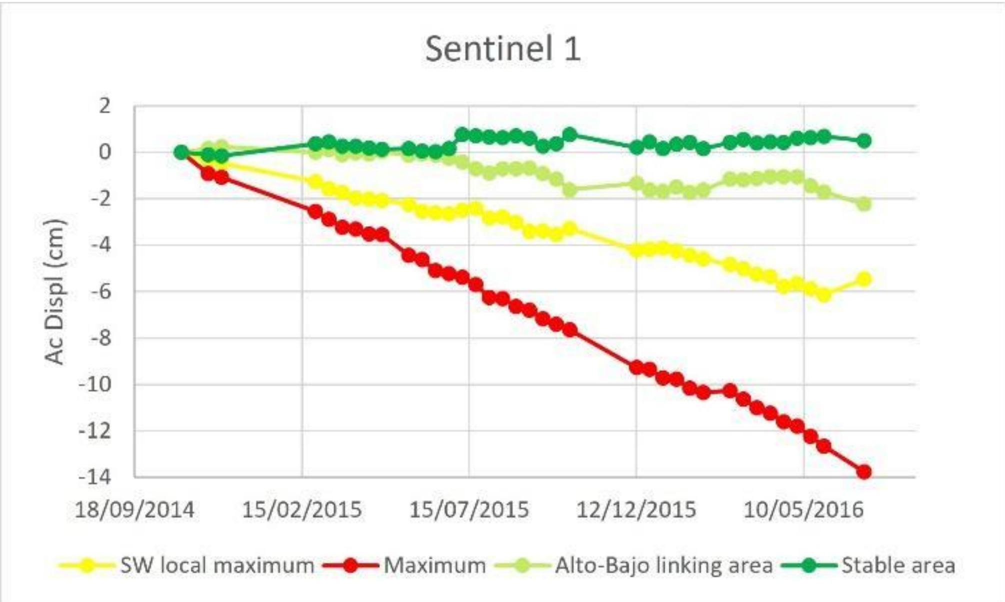

Figure 6.2 Accumulated LOS displacements during the S-1 dataset time span (30/10/2014-03/07/2016). In red, representative TS of maximum subsidence area. In yellow the SW local maximum towards Puerto Lumbreras. In light green, representative TS of the linking area between the Alto Guadalentín and Bajo Guadalentín (upper and lower sections of the Guadalentín basin). In dark green, representative TS of a stable area located in the West.

6.2 CSK Analysis results

Figure 6.3 shows the InSAR map of deformation rates derived from CSK processing. The measurements are in LOS with an angle of 43.16º from the normal to the Earth's surface. As well as for S1 dataset, a ±1 cm/year was used as the stability threshold. The deformation pattern is similar to that obtained with the S-1 dataset, detecting the maximum deformation at the northern area of the basin. The maximum deformation rate in LOS was -8.2 cm/year (movement away from the satellite). If only vertical displacement is considered, the vertical projected maximum velocity rises up to -11.1 cm/year. The accumulated deformation is higher than that derived from S-1 data. Representative TS of the deformation areas classified in Figure 6.3 are displayed in Figure 6.4.

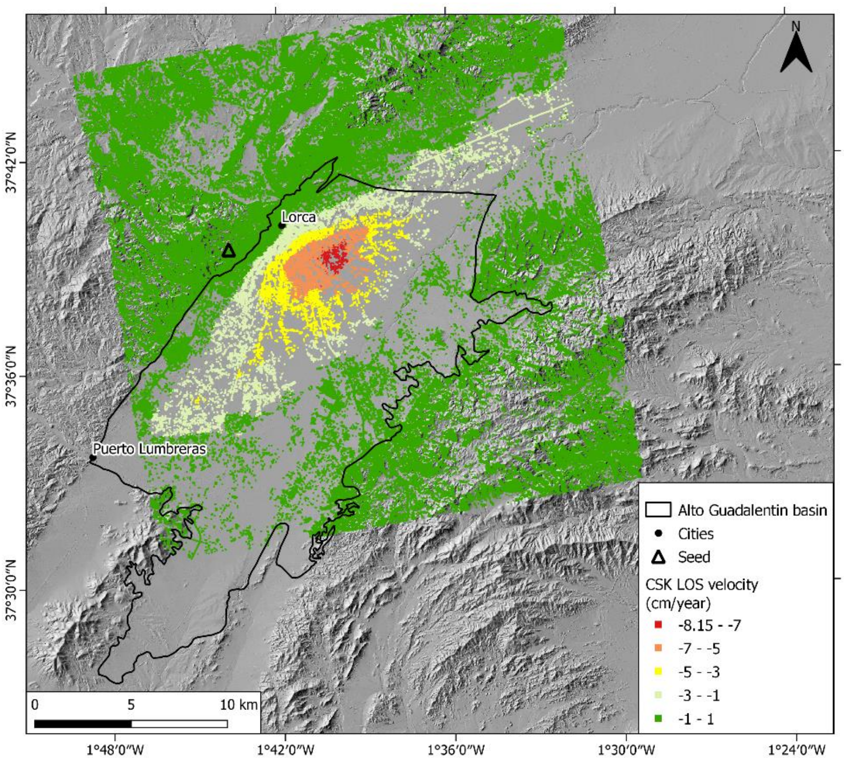

Figure 6.3 LOS displacement velocity in the study area for the CSK dataset processed with CPT. Period June 2011 to December 2016.

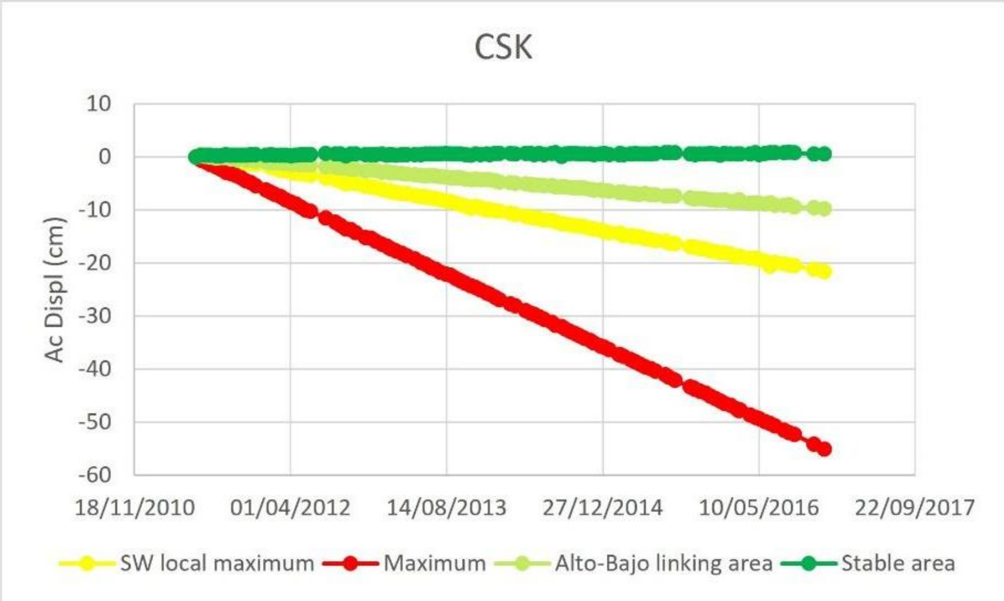

Figure 6.4 Accumulated LOS displacements during the CSK dataset time span (02/06/2011 – 05/12/2016). In red, a representative TS of maximum subsidence area. In yellow the SW local maximum towards Puerto Lumbreras. In light green, representative TS of the linking area between the Alto Guadalentín and Bajo Guadalentín (upper and lower sections of the Guadalentín basin). In dark green, representative TS of a stable area located in the West.

6.3 Comparison between datasets

For the Alto Guadalentín study area additional satellite data from CSK satellite has been processed besides S-1. It should be noted that for the rest of the pilot sites only S-1 data will be processed by A-DInSAR techniques. The two datasets overlap each other spatially and cover almost the whole extent of the aquifer boundary (Figure 6.5). A time span of more than 5 years of surface displacements are available. However, the datasets have different viewing geometries that must be considered for further analysis and interpretation (Table 6.1). There is the possibility of decomposing the LOS displacements into up-down and east-west components from ascending CSK and descending S1 data, which overlap in time, by interpolating the displacement rate to a common resolution grid (Ezquerro et al., 2020).

In general terms, there is a spatial good fit between the datasets of the maximum deformation area, which is located in the northern section of the aquifer (Figure 6.6). Again, for an accurate interpretation it has to be considered that individual datasets measures are a one-dimensional motion along the radar LOS and that each satellite has a different incidence angle, orbit mode and resolution.

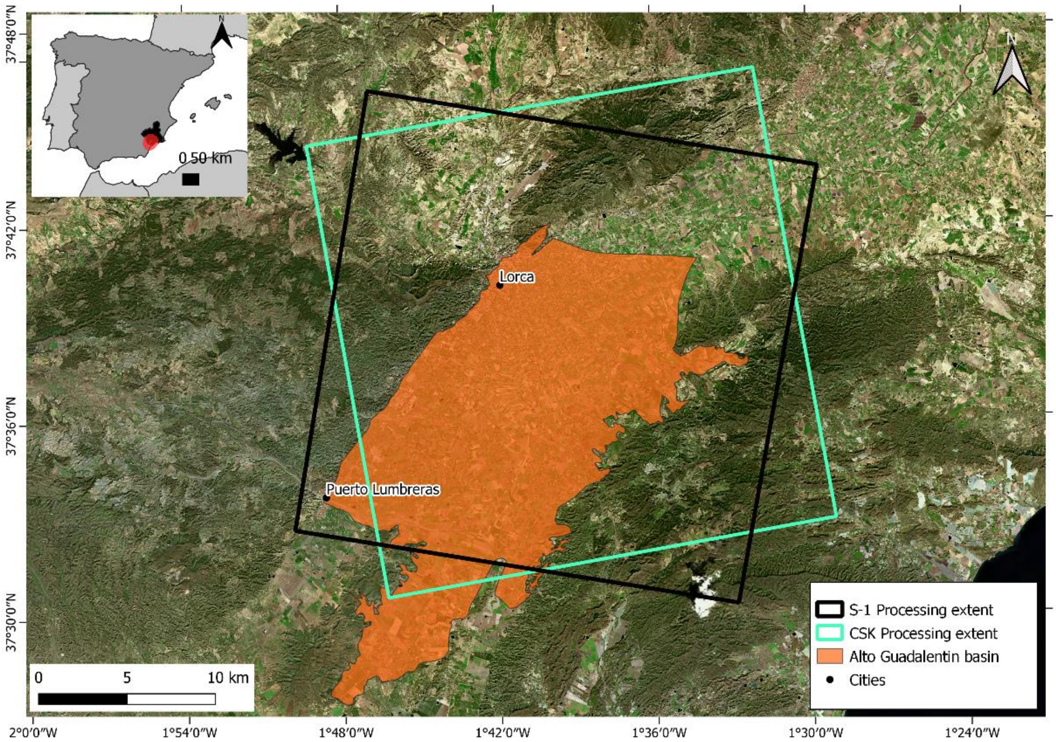

Figure 6.5 Extents of S-1 and CSK datasets processed with CPT.

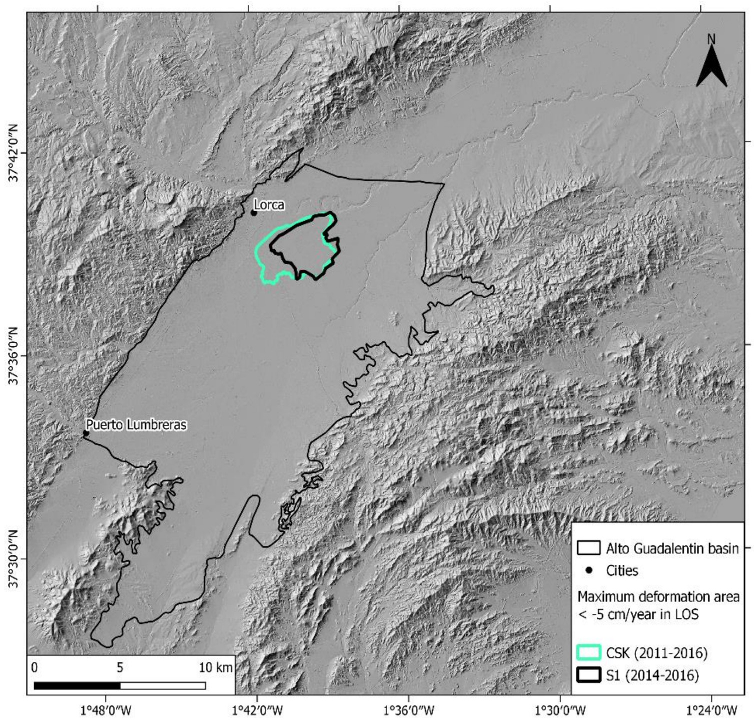

Figure 6.6 Maximum deformation areas (more than -5cm/year of LOS velocity away from the satellite) of the two datasets processed with CPT. Note that the incidence angle (angle between the LOS of the radar sensor and the normal to the Earth surface) is different for each satellite.

Table 6.1 Main characteristics of the two datasets available for the studied area.

	S-1	CSK
Period	30/10/2014-03/07/2016	02/06/2011-05/12/2016
SAR images	37	114
Band	C	X
Orbit	Descending	Ascending
Incidence angle	37.54º - 39.08º	43.16º
Area processed [km^2]	625	676
Spatial resolution after ML (az × rg)	45 × 45	25 × 25
Number of DS points	206,530	422,458
DS density [DS per km^2]	330	625
A-DInSAR technique	CPT	CPT

7 CONCLUSIONS

This report presents the A-DInSAR processing results of the Alto Guadalentín study area using two different SAR datasets from Sentinel-1 (S-1) and Cosmo Sky-Med (CSK) satellites.

The document firstly introduces the general features of S-1 products and the A-DInSAR techniques that will be applied in all the studied areas to retrieve surface displacements. Secondly, a preliminary deformation map at a regional scale was generated using the unsupervised P-SBAS interferometric chain implemented in GEP, with 79 S-1 SAR images acquired in the period July 2017 to November 2018. After that, a more refined and accurate processing of the Alto Guadalentín pilot site using the CPT algorithm is detailed. The CPT local processing was performed using 37 SAR images acquired between October 2014 to July 2016. We deliver the surface displacements results obtained with the CPT in a shapefile format (point features), along with other geographic vector and raster data to generate a descriptive map in a Geographic Information System (GIS). This document also describes, presents and delivers the surface displacements obtained with CSK dataset and processed with the CPT, which is constituted by 114 SAR images acquired between June 2011 to December 2016. Displacements and velocities are given in LOS. Lastly, a brief analysis of the results is given for each SAR dataset, along with a comparison between them. The maximum deformation area obtained by both datasets coincide at the northern section of the basin and the maximum rates detected in LOS were –7.5 cm/year and -11.1 cm/year, from S-1 and CSK datasets respectively.

REFERENCES

Béjar-Pizarro, M., Guardiola-Albert, C., García-Cárdenas, R. P., Herrera, G., Barra, A., López Molina, A., Tessitore, S., Staller, A., Ortega-Becerril, J. A., and García-García, R. P., 2016, Interpolation of GPS and geological data using InSAR deformation maps: Method and application to land subsidence in the alto guadalentín aquifer (SE Spain): Remote Sensing, v. 8, no. 11, p. 965.

Berardino, P., Fornaro, G., Lanari, R., and Sansosti, E., 2002, A new algorithm for surface deformation monitoring based on small baseline differential SAR interferograms: Geoscience and Remote Sensing, IEEE Transactions on, v. 40, no. 11, p. 2375-2383.

Blanco-Sanchez, P., Mallorquí, J. J., Duque, S., and Monells, D., 2008, The coherent pixels technique (CPT): An advanced DInSAR technique for nonlinear deformation monitoring: Pure and Applied Geophysics, v. 165, no. 6, p. 1167-1193.

Bonì, R., Herrera, G., Meisina, C., Notti, D., Béjar-Pizarro, M., Zucca, F., González, P. J., Palano, M., Tomás, R., and Fernández, J., 2015, Twenty-year advanced DInSAR analysis of severe land subsidence: The Alto Guadalentín Basin (Spain) case study: Engineering Geology, v. 198, p. 40-52.

Bovenga, F., Wasowski, J., Nitti, D., Nutricato, R., and Chiaradia, M., 2012, Using COSMO/SkyMed X-band and ENVISAT C-band SAR interferometry for landslides analysis: Remote Sensing of Environment, v. 119, p. 272-285.

Casu, F., Elefante, S., Imperatore, P., Zinno, I., Manunta, M., De Luca, C., and Lanari, R., 2014, SBAS-DInSAR parallel processing for deformation time-series computation: IEEE Journal of Selected Topics in Applied Earth Observations and Remote Sensing, v. 7, no. 8, p. 3285-3296.

Centolanza, G., Duro, J., and Mallorquí, J., Achieving precise Sentinel 1 coregistration with CPT, experience and lesson learnt, *in* Proceedings Proceedings of the Fringe 2017 Workshop, Helsinky, Finland2017, p. 5-9.

Covello, F., Battazza, F., Coletta, A., Lopinto, E., Fiorentino, C., Pietranera, L., Valentini, G., and Zoffoli, S., 2010, COSMO-SkyMed an existing opportunity for observing the Earth: Journal of Geodynamics, v. 49, no. 3-4, p. 171-180.

Crosetto, M., Monserrat, O., Cuevas-González, M., Devanthéry, N., and Crippa, B., 2016, Persistent scatterer interferometry: A review: ISPRS Journal of Photogrammetry and Remote Sensing, v. 115, p. 78-89.

De Luca, C., Cuccu, R., Elefante, S., Zinno, I., Manunta, M., Casola, V., Rivolta, G., Lanari, R., and Casu, F., 2015, An on-demand web tool for the unsupervised retrieval of earth's surface deformation from SAR data: The P-SBAS service within the ESA G-POD environment: Remote Sensing, v. 7, no. 11, p. 15630-15650.

ESA-web, https://sentinel.esa.int/web/sentinel/missions/sentinel-1. *Accessed 16/12/2020*

Ezquerro, P., Tomás, R., Béjar-Pizarro, M., Fernández-Merodo, J., Guardiola-Albert, C., Staller, A., Sánchez-Sobrino, J., and Herrera, G., 2020, Improving multi-technique monitoring using Sentinel-1 and Cosmo-SkyMed data and upgrading groundwater model capabilities: Science of The Total Environment, v. 703, p. 134757.

Flores-Anderson, A. I., Herndon, K. E., Thapa, R. B., and Cherrington, E., 2019, The SAR Handbook: Comprehensive Methodologies for Forest Monitoring and Biomass Estimation.

Mallorquí, J. J., Mora, O., Blanco, P., and Broquetas, A., Linear and non-linear long-term terrain deformation with DInSAR (CPT: Coherent Pixels Technique), *in* Proceedings Proc. of FRINGE 2003 Workshop. ESA2003, p. 1-8.

Minh, D. H. T., Hanssen, R., and Rocca, F., 2020, Radar Interferometry: 20 Years of Development in Time Series Techniques and Future Perspectives: Remote Sensing, v. 12, no. 9, p. 1364.

Mora, O., Mallorqui, J. J., and Broquetas, A., 2003, Linear and nonlinear terrain deformation maps from a reduced set of interferometric SAR images: IEEE Transactions on Geoscience and Remote Sensing, v. 41, no. 10, p. 2243-2253.

Osmanoğlu, B., Sunar, F., Wdowinski, S., and Cabral-Cano, E., 2016, Time series analysis of InSAR data: Methods and trends: ISPRS Journal of Photogrammetry and Remote Sensing, v. 115, p. 90-102.

UNAVCO, https://www.unavco.org/instrumentation/geophysical/imaging/sar-satellites/sar-satellites.html. *Accessed 16/12/2020.*